Kinetic Study of the Catalytic Mechanism of Mannitol Dehydrogenase from *Pseudomonas fluorescens*†

Matthias Slatner,‡ Bernd Nidetzky,*,‡ and Klaus D. Kulbe

Division of Biochemical Engineering, Institute of Food Technology, Universität für Bodenkultur Wien (BOKU), Muthgasse 18, A-1190 Wien, Austria

Received February 10, 1999; Revised Manuscript Received May 21, 1999

ABSTRACT: To characterize catalysis by NAD-dependent long-chain mannitol 2-dehydrogenases (MDHs), the recombinant wild-type MDH from *Pseudomonas fluorescens* was overexpressed in *Escherichia coli* and purified. The enzyme is a functional monomer of 54 kDa, which does not contain Zn^{2+} and has B-type stereospecificity with respect to hydride transfer from NADH. Analysis of initial velocity patterns together with product and substrate inhibition patterns and comparison of primary deuterium isotope effects on the apparent kinetic parameters, $^{D}k_{cat}$, $^{D}(k_{cat}/K_{NADH})$, and $^{D}(k_{cat}/K_{fructose})$, show that MDH has an ordered kinetic mechanism at pH 8.2 in which NADH adds before D-fructose, and D-mannitol and NAD are released in that order. Isomerization of E−NAD to a form which interacts with D-mannitol nonproductively or dissociation of NAD from the binary complex after isomerization is the slowest step ($\geq$110 s^{-1}) in D-fructose reduction at pH 8.2. Release of NADH from E−NADH (32 s^{-1}) is the major rate-limiting step in mannitol oxidation at this pH. At the pH optimum for D-fructose reduction (pH 7.0), the rate of hydride transfer contributes significantly to rate limitation of the catalytic cascade and the overall reaction. $^{D}(k_{cat}/K_{fructose})$ decreases from 2.57 at pH 7.0 to a value of $\leq$1 above pH 9.6, corresponding to the p*K* of 9.34 observed in the pH profile of $k_{cat}/K_{fructose}$. Therefore, hydride transfer is not pH-dependent, and D-fructose is not sticky at pH 7.0. A comparison of the kinetic data of MDH and mammalian sorbitol dehydrogenase, presumably involved in detoxification metabolism, is used to point out a physiological function of MDH in the oxidation of D-mannitol with high specificity and fluxional efficiency under prevailing reaction conditions in vivo.

The six-carbon polyalcohol D-mannitol is widely distributed in nature and serves a broad range of different functions. It can be utilized as a carbon source for growth and energy, a carbon storage compound, a free radical scavenger, or a compatible solute providing protection against various forms of stress (*1*). The initial step in the catabolism of D-mannitol involves oxidations at the C-1 (*2*, *3*) and C-2 (*4*−*6*) positions, catalyzed by NAD(P)-dependent dehydrogenases. The reaction catalyzed by mannitol 2-dehydrogenase (MDH,[1] EC 1.1.1.67) is

$$\text{D-mannitol} + NAD^+ \leftrightarrow \text{D-fructose} + NADH + H^+ \quad (1)$$

At present, there is little known about the structure−function relationships of MDH, and the kinetic and chemical mechanisms of MDH have not been studied, except for an early kinetic study with the MDH from the fungus *Absidia glauca* (*7*). The primary structures of three microbial MDHs from *Pseudomonas fluorescens* (*8*), *Rhodobacter sphaeroides* (*9*), and *Rhodobacter capsulatus* (GenBank accession number gi|3128349) have been determined together with those of hypothetical proteins in *Saccharomyces cerevisiae* and *Escherichia coli*. However, only the enzymes from *P. fluorescens* (*10*) and *Rh. sphaeroides* (*11*) have been characterized at the protein level in some detail. The sequences of the MDHs are ≈40% similar to each other and ≈20% similar to those of other members of the mannitol dehydrogenase family (*9*), which so far includes MDHs, mannitol 1-phosphate dehydrogenases, mannonate dehydrogenases or fructuronate reductases (EC 1.1.1.57), tagaturonate reductases (EC 1.1.1.58), and probably D-xylulose-forming D-arabinitol dehydrogenases from bacteria and yeast. Overall similarities to other functionally related enzyme families such as the zinc-containing medium-chain dehydrogenases (*12*, *13*), short-chain dehydrogenases/reductases (SDR; *14*, *15*), or aldo/keto reductases (AKR; *16*) are not significant (*9*). With molecular masses of the protein subunit of about 54 kDa, the MDHs belong to the family of long-chain dehydrogenases (*9*), and typically, significant entire-chain identities are not detected for different members of this heterogeneous family (*17*, *18*).

In this paper, we present a detailed kinetic study of the catalytic mechanism of the MDH from *P. fluorescens*. The work was undertaken for two reasons. First of all, bacterial

† Supported by FFF Project Enzymatic Reduction of Disaccharides and a project of the Austrian Science Fund (P-12569-MOB).

* To whom correspondence should be addressed: Institute of Food Technology, Universität für Bodenkultur (BOKU), Muthgasse 18, A-1190 Wien, Austria. Phone: +43-1-36006-6274. Fax: +43-1-36006-6251. E-mail: nide@mail.boku.ac.at.

‡ These authors contributed equally to this work.

[1] Abbreviations: MDH, mannitol 2-dehydrogenase (D-mannitol:NAD 2-oxidoreductase, EC 1.1.1.67); SDH, sorbitol 2-dehydrogenase (L-iditol:NAD 2-oxidoreductase, EC 1.1.1.14); SDR, short-chain dehydrogenases/reductases; MDH-H_6, MDH with a C-terminal hexahistidine metal affinity tag; wt-MDH, recombinant wild-type MDH.

10.1021/bi990327g CCC: $18.00
Published on Web 07/22/1999

MDHs are presumed to have a key function in the mainstream catabolism of D-mannitol, and the kinetic parameters for MDH are expected to reflect this physiological role, at least to some extent. As a frame of reference for analyzing the kinetic properties of MDH, we have chosen the sorbitol dehydrogenase (SDH) from sheep liver which in contrast to MDH does not act in a "high-flux" metabolic route and is a broad spectrum polyol dehydrogenase, presumably involved in cellular detoxification metabolism (*19*−*21*). The results show that at prevailing concentrations of NAD and NADH, MDH has evolved to function with high fluxional efficiency in the oxidation of D-mannitol (to D-fructose) and probably D-arabinitol (to D-xylulose), but not that of other polyols. Thus, the kinetic data clearly reflect the functional differences between MDH and SDH.

Initial velocity studies together with isotope effect and pH studies have been used to elucidate the kinetic and chemical mechanisms of NAD(P)-dependent enzymes (for review, see ref *22*) which like MDH, catalyze carbonyl−alcohol interconversions (*23*−*29*). To characterize the kinetic mechanism of MDH, particularly that in D-fructose reduction, was the second aim of this work. The results show that MDH utilizes the 4-*pro*-*S* hydrogen of NADH to reduce D-fructose in a *si* side attack, thus forming D-mannitol. Polarization of the substrate carbonyl group prior to or in concert with the hydride transfer step is achieved without participation of a divalent metal ion. MDH has an ordered kinetic mechanism, and reaction steps for nucleotide exchange are partially rate-limiting in the forward and reverse reaction (eq 1). At the pH optimum for reduction, the rates of hydride transfer and proton transfer contribute significantly to rate limitation of the catalytic cascade ($k_{cat}/K_{fructose}$) as well as the overall reaction (k_{cat}) catalyzed by MDH.

MATERIALS AND METHODS

Materials. The material for chromatography and electrophoresis was from Amersham Pharmacia. All chemicals and reagents were of the highest purity available from Sigma. D_2O contained 99% deuterium. D-Xylulose was prepared from D-arabinitol by microbial oxidation with resting cells of *Gluconobacter* sp. (*30*). Typically, 300 mM D-arabinitol was incubated with 10 g/L washed bacterial cells for about 10 h at 25 °C [50 mM potassium phosphate (pH 7.0)]. The thus obtained D-xylulose contained less than 1% residual D-arabinitol. Prior to use in kinetic studies, it was gel filtered and lyophilized. D-*Arabino*-hexosulose (D-glucosone) was prepared by reported methods using pyranose 2-oxidase (*31*). Stereospecifically deuterium-labeled (4*R*)-[4-D]NADD and (4*S*)-[4-D]NADD were prepared using yeast alcohol dehydrogenase and 2-propanol-d_8, and glucose dehydrogenase (Amano) and D-glucose-d_1, respectively (*32*). The deuterated nucleotides were purified by MonoQ anion-exchange chromatography on an FPLC system according to the method of Orr and Blanchard (*33*).

Enzyme Production, Purification, and Characterization. Recombinant wild-type MDH from *P. fluorescens* DSM 50106 and a variant enzyme form (MDH-H_6) which has a C-terminal hexahistidine metal affinity tag were overexpressed in *E. coli* strain JM 109 as previously described (*8*). The expression plasmids were pETR 127 and pETR241 for MDH and MDH-H_6, respectively (*8*). MDH was purified by two successive steps of anion-exchange chromatography using a 8 cm × 2.6 cm column of DEAE-Sepharose, equilibrated with 50 mM Tris/HCl buffer (pH 7.0). Protein elution in both steps was accomplished at a flow rate of 50 cm/h by using a linear gradient of 0.0 to 0.5 M NaCl, and MDH eluted at 0.1 M NaCl. The MDH-containing fractions of the first ion-exchange step were gel filtered (Sephadex G25) prior to rechromatography on DEAE-Sepharose. MDH-H_6 was purified by immobilized metal affinity chromatography (IMAC) as previously described (*8*), the exception being that a 3 cm × 2.6 cm copper-loaded chelating Sepharose Fast Flow column was used. MDH and MDH-H_6 were gel filtered on P-10 columns, and enzyme stock solutions with concentrations of approximately 5 mg/mL were prepared by concentration in Millipore ultrafiltration centrifugal tubes. During chromatography, purification was monitored by the measurement of specific enzyme activity as well as SDS−polyacrylamide gel electrophoresis using an ExcelGel (8 to 18%) on a Pharmacia Multiphore system. The p*I* of MDH was determined using a Phastgel IEF 3-9 on a Pharmacia Phastsystem. The apparent molecular mass of native MDH was determined by gel filtration on Superose 12 (1.5 cm × 30 cm) using 50 mM Tris/HCl buffer (pH 7.0) containing 0.5 M NaCl, and protein elution was performed at a flow rate of 0.5 mL/min.

Metal Analysis. The metal content (Zn^{2+} and Mg^{2+}) of MDH was determined by high-resolution inductively coupled plasma mass spectrometry on a Finnigan MAT instrument (Bremen, Germany), described elsewhere in detail (*34*). MDH was gel filtered three times with ultrapure MilliQ water before the analysis. The enzyme sample contained 1 mg of protein/mL. MilliQwater was used as the blank.

Assay Conditions. Unless otherwise noted, all kinetic measurements and assays were carried out in 50 mM Tris/HCl buffer (pH 7.0), at a constant temperature of 25 ± 0.5 °C, by using a Beckman DU-650 spectrophotometer and measuring at 340 nm the rate of appearance of NAD(P)H in the direction of D-mannitol oxidation and the rate of disappearance of NAD(P)H in the direction of D-fructose reduction. The standard mixture for assaying MDH activity contained 200 mM D-fructose and 0.2 mM NADH, and 1 MDH unit (U) refers to 1 μmol of NADH consumed per minute. Initial velocity data were obtained under conditions in which one substrate was varied at several constant concentrations of the second substrate.

The pH profile for NADH-dependent D-fructose reduction was determined over the pH range of 6.5−10.0 using a buffer mixture of 50 mM Tris/HCl and 50 mM sodium citrate. For the pH studies, D-fructose was the varied substrate, and NADH was constant at 0.20 mM ($\approx 2K_{NADH}$), which was the highest nucleotide concentration that is compatible with the spectrophotometric assay and is approximately 65% saturating. Therefore, the true values for k_{cat} and $k_{cat}/K_{fructose}$ could not be determined under these conditions. Since NADH is the first substrate in D-fructose reduction by MDH (see the Results), the thus obtained apparent k_{cat} values are $k_{cat}/(1 + K_{NADH}/[NADH])$, and the apparent $k_{cat}/K_{fructose}$ values are $(k_{cat}/K_{fructose})/(1 + K_{iNADH}/[NADH])$. The pH profiles of k_{cat} and $k_{cat}/K_{fructose}$ are valid unless K_{NADH} and K_{iNADH} change in the pH range that was studied. It was proven that the decrease in k_{cat} at high and low pH was not due to the instability of MDH.

Kinetic parameters for several alternate polyol and ketose substrates of MDH were determined at a constant saturating concentration of NAD ($\approx 10K_{NAD}$) and at 0.20 mM NADH (see above). In the direction of ketose reduction, the reported values for k_{cat} and k_{cat}/K_{ketose} are apparent because they are uncorrected for the incomplete saturation of MDH with nucleotide. Kinetic parameters for NAD(P) and NAD(P)H were determined at constant concentrations of D-mannitol and D-fructose, respectively. The NAD(P)H concentration range was 0.005−0.20 mM.

Primary deuterium isotope effects on apparent kinetic parameters were obtained by using (4*S*)-[4-D]NADD. The deuterium solvent isotope effect on $k_{cat}/K_{fructose}$ was measured by direct comparison of initial velocities at a constant NADH concentration (0.2 mM). It was taken into account that the level of saturation of MDH with NADH could be different in H_2O and D_2O, and therefore, the solvent isotope effect on k_{cat} was confirmed by direct comparison of initial velocities with varied NADH concentrations at a constant level of D-fructose (150 mM) which is the highest noninhibitory concentration of the ketose. Buffers with D_2O were brought to "pH" with DCl using correction for the isotope effect on the response of the pH electrode according to the relation pD = meter reading + 0.4.

Data Processing. Reciprocal initial velocities were plotted versus reciprocal substrate concentrations, and the experimental data were fitted to eqs 2−9 by the least-squares method

$$v = k_{cat}EA/(K + A) \quad (2)$$

$$v = k_{cat}EA/(K + A + A^2/K_I) \quad (3)$$

$$v = k_{cat}EAB/(K_{ia}K_b + K_aB + K_bA + AB + AB^2/K_I) \quad (4)$$

$$v = k_{cat}EA/[K(1 + F_iE_{V/K}) + A(1 + F_iE_V)] \quad (5)$$

$$v = k_{cat}EA/[K(1 + I/K_{is}) + A] \quad (6)$$

$$v = k_{cat}EA/[K(1 + I/K_{is}) + A(1 + I/K_{ii})] \quad (7)$$

$$v = k_{cat}EA/[K + A(1 + I/K_{ii})] \quad (8)$$

$$\log Y = \log[C/(1 + K_1/H)] \quad (9a)$$

$$\log Y = \log[C/(1 + H/K_1 + K_2/H)] \quad (9b)$$

$$\log Y = \log\{[Y_L + Y_H(K_1/H)]/(1 + K_1/H)\} \quad (9c)$$

assuming equal variances for the v and log Y values, and using the Sigmaplot program version 5 for Windows (Jandel). The correlation coefficient of regression analysis was generally >0.985, and problems with strongly correlated parameter estimates were not observed. Figures show the experimentally determined values, and curves are calculated from fits of the data to the appropriate equation. Linear double-reciprocal plots were fitted to eq 1, and eq 2 was employed when substrate inhibition was observed. Equation 3 describes an intersecting initial velocity pattern with uncompetitive substrate inhibition by *B*. Equation 4 was used to determine the kinetic deuterium isotope effects and the solvent deuterium isotope effects when one substrate was varied, where $E_{V/K}$ and E_V are the isotope effects minus 1 on k_{cat}/K and k_{cat}, respectively. The fraction of deuterium in the labeled substrate is given by F_i. Equations 6−8 were used when linear competitive, linear noncompetitive, and uncompetitive product inhibition were observed, respectively. The pH profiles were fitted to eqs 9a and 9b, which describe log Y versus pH curves, which are level below pK_1 but decrease with a slope of −1 above pK_1 (eq 9a), decrease below pK_1 and above pK_2 (eq 9b), and exhibit two plateaus with pK_1 being the point where Y is the average of the two plateau values (eq 9c). In eqs 9a−c, H is [H^+] and C is the pH-independent value of Y at the optimal state of protonation.

Stereospecificity of the Hydride Transfer. This was studied by ^{1}H NMR, performed with a Bruker Avance 300 NMR unit at 300 MHz. Spectra were recorded at 27 °C using D_2O (99%) and 3-(trimethylsilyl)-1-propanesulfonic acid (sodium salt) as the reference. The deuterium content of (4*R*)-[4-D]-NADD and (4*S*)-[4-D]NADD was determined to be greater than 98%. A typical reaction mixture contained 2 mg of (4*R*)-[4-D]NADD or (4*S*)-[4-D]NADD, 3 U of MDH, and 100 mM D-fructose dissolved in 50 mM potassium phosphate buffer (pD 7.0). When the oxidation of NADD was complete (monitored spectrophotometrically at 340 nm), the sample was used for NMR analysis without further treatment. The stereospecificity for the hydride transfer for MDH was determined by comparing the integrated peak area of C4-H (δ 8.75 ppm) for the reaction mixtures containing B- or A-side-labeled NADH as the coenzyme.

NADH Binding. To determine the NADH binding constant of MDH, the enhancement of the nucleotide fluorescence on binding to MDH was followed by using a Hitachi F-2000 spectrofluorometer with a thermostated cell compartment (25 ± 0.5 °C). The fluorescence titrations were carried out at a MDH concentration of 0.3 mg/mL in 50 mM Tris/HCl buffer (pH 7.0). Fluorescence measurements were taken after adding a 5 μL aliquot from a 1.00 mM NADH stock solution in buffer to the protein by recording the emission wavelength spectrum between 390 and 550 nm (5 nm bandwidth) using an excitation wavelength of 360 nm (5 nm bandwidth). Controls were obtained by the same procedure without enzyme, and corrections for the blank values at the corresponding NADH concentrations were made in all cases. Scatchard analysis was used to determine the number of NADH binding sites in MDH and the dissociation constant of the MDH−NADH complex.

RESULTS

Functional Characterization of MDH. Recombinant wild-type MDH (wt-MDH) and MDH-H_6 were purified to homogeneity in yields of 40 and 70% (*8*), respectively, judging by the criterion of SDS−polyacrylamide gel electrophoresis in which both enzyme preparations migrated as single protein bands with an apparent molecular mass of 54 kDa. The apparent molecular masses of native wt-MDH and MDH-H_6 were determined by Superose12 gel filtration and are 45 ± 5 kDa. Hence, the enzymes are functional monomers. Upon isolelectric focusing, wt-MDH and MDH-H_6 exhibited one single band with p*I* values of 4.5 and 4.8, respectively. The p*I* of the recombinant wt-MDH agrees with the p*I* determined for MDH isolated from *P. fluorescens* (not shown). The apparent kinetic parameters for wt-MDH and MDH-H_6 in the direction of D-mannitol oxidation and

Table 1: Apparent Kinetic Parameters for MDH[a]

parameter[b]	NAD(H)	NADP(H)
k_{catr} (s^{-1})[c]	54 (56)[d]	3.4 (≈19)[d,e]
$k_{catr}/K_{fructose}$ (mM^{-1} s^{-1})	2.2	0.02
$k_{catr}/K_{NAD(P)H}$ (mM^{-1} s^{-1})	436[f]	≈20[f]
$K_{Ifructose}$ (M)	0.72	nd[g]
k_{cato} (s^{-1})	20	1.1
$k_{cato}/K_{mannitol}$ (mM^{-1} s^{-1})	18	0.03
$k_{cato}/K_{NAD(P)}$ (mM^{-1} s^{-1})	159	1.2
$K_{Imannitol}$ (M)	1.36	nd[g]

[a] Kinetic parameters were obtained from fits to eq 2, by using initial velocities determined at 25 °C in 50 mM Tris/HCl buffer at pH 7.0 (D-fructose reduction) and 9.0 (D-mannitol oxidation). [b] Unless noted (≈), the standard errors for parameters are less than 15%. [c] Determined from initial velocity data when the D-fructose concentration was varied in the range of 5−500 mM and the NAD(P)H concentration was constant at 0.2 mM. [d] In parentheses, determined from initial velocity data when the NAD(P)H concentration was varied and the D-fructose concentration was constant at 150 mM. [e] With NADPH, MDH requires coenzyme concentrations of >2 mM for saturation. [f] Calculated by using k_{catr} values in parentheses. [g] Not detectable.

D-fructose reduction were identical within experimental error. The pH dependence of the enzyme activity in either direction of reaction was identical, revealing pH optima of 7.0 for D-fructose reduction and 10.0 for D-mannitol oxidation, so both enzymes are kinetically indistinguishable. Therefore, the MDH-H_6 was employed in all further kinetic experiments because it was easier to obtain as a homogeneous protein.

Metal Analysis. The primary structure of MDH provides no evidence of a putative zinc-binding site like that found in medium-chain alcohol dehydrogenases (*35*) or sorbitol dehydrogenases (*36*). However, given the low entire-chain sequence similarity of MDH with zinc-containing alcohol/sorbitol dehydrogenase (<20%; *9*), a metal site may not be detected easily by sequence comparison. We therefore determined the metal content (Zn^{2+} and Mg^{2+}) of purified wt-MDH, by using high-resolution inductively coupled plasma mass spectrometry. MDH is not a metal enzyme. It is resistant to metal chelators such as EDTA (1−4 mM, pH 7.5).

MDH Has a Dual Coenzyme Specificity. MDH exhibits a strong preference for NAD(H), relative to NADP(H), but significant enzyme activity is observed with NADP(H). A comparison of the apparent kinetic parameters of MDH determined with NAD(H) and NADP(H) as coenzymes is shown in Table 1. A preference of MDH for NAD(H), relative to NADP(H), is manifested by large decreases in the catalytic constants (16−18-fold) and increases in the apparent Michaelis constants for both the coenzyme and substrate. Judging from a comparison of the specificity constants (k_{cat}/K) according to

$$\Delta\Delta G = -RT \ln[(k_{cat}/K)_{NADP(H)}/(k_{cat}/K)_{NAD(H)}] \quad (10)$$

a loss of binding energy of 7.4 and 12.1 kJ/mol occurs at the level of the binary MDH−NADPH and MDH−NADP complex, respectively, and 11.6 and 15.3 kJ/mol at the level of the ternary MDH−NADPH−D-fructose and MDH−NADP−D-mannitol complex, respectively. We show below that MDH has an ordered kinetic mechanism in which the coenzyme binds first and leaves last.

Polyol and Ketose Substrates of MDH. In addition to D-mannitol, few other polyols exhibit productive interaction with the binary MDH−NAD complex and are converted into the corresponding ketoses by MDH (Table 2). Noncovalent interactions of the polyol and ketose substrate with the MDH−NAD and MDH−NADH complexes, respectively, are found to be important for (i) transition state stabilization, reflected by k_{cat}/K, and (ii) a reduction of the activation energy for the rate-limiting step, reflected by k_{cat}. The values for k_{cat}/K span more than 2 log units, reflecting an approximately 7-fold variation in k_{cat} and an approximately 300-fold variation in $K_{substrate}$. In other words, the binding energy derived from noncovalent enzyme−substrate interactions contributes at least ≈16 kJ/mol to transition state stabilization, comparing the k_{cat}/K values for D-mannitol and D-sorbitol. MDH requires that the polyol/ketose have at least five carbon atoms to be a substrate which is converted at appreciable reaction rates (Figure 1). For C-6 ketoses, the D-*arabo* configuration in D-fructose is preferred over the L-*xylo* configuration in L-sorbose, whereas for C-5 ketoses, the D-*erythro* configuration in D-ribulose is preferred over the D-*threo* configuration in D-xylulose (cf. Figure 1). D-Psicose, D-sorbose, and D-tagatose are no C-6 ketose substrates of MDH. No enzyme activity (<1%) was observed with a dicarbonyl substrate such as D-glucosone. For polyol substrates, the presence of the D-*arabo* configuration is required, and with six carbon polyols, the C-2 (*R*) configuration is preferred, comparing D-mannitol with D-sorbitol, C-2 (*S*). MDH is completely inactive with D-fructose 6-phosphate and D-mannitol 1-phosphate in directions of carbonyl reduction and polyol oxidation, respectively.

Stereospecificity of Hydride Transfer from NADH. When (4*R*)-[4-D]NADD is used as a coenzyme for reduction of D-fructose, the (4*S*) hydrogen is depleted upon MDH-catalyzed oxidation of NADD. By contrast, when (4*S*)-[4-D]NADD is used, the deuterium is depleted at the C-4 position of the nicotinamide ring. Therefore, MDH is a B-type specific dehydrogenase which transfers the 4-*pro*-*S* hydrogen in a *si* side attack to the carbonyl group of D-fructose, thus producing specifically D-mannitol, and not D-sorbitol.

Initial Velocity Patterns at pH 8.2. The forward reaction, oxidation of D-mannitol (eq 1), and the reverse reaction exhibit sequential kinetics (intersecting patterns) with uncompetitive substrate inhibition by D-mannitol and D-fructose, respectively, causing the double-reciprocal plots to become parallel at high substrate concentrations. The data were fitted to eq 4, and the kinetic constants are summarized in Table 3.

Haldane Relationship. The internal consistency of the kinetic constants in Table 3 was checked with the kinetic Haldane relationship for an ordered bi bi mechanism:

$$\text{app } K_{eq} = (k_{cat}/K_{mannitol})K_{iNADH}/[(k_{cat}/K_{fructose})K_{iNAD}] \quad (11)$$

where app K_{eq} is the apparent equilibrium constant for eq 1 at pH 8.2.

The kinetic constants in Table 3, using a value for $K_{fructose}$ without correction for the free carbonyl species in aqueous solution, which is then 63 mM, give a value of 1.30 for this expression. This value corresponds to a thermodynamic K_{eq} value of 8.2×10^{-9} M and agrees with the experimentally observed value of 5.3×10^{-9} M. In Table 3, the inverse apparent equilibrium constant, 1/app K_{eq}, is given. The free carbonyl form of D-fructose (≈1%; *37*) will probably be the

Table 2: Substrate Spectrum of MDH from *P. fluorescens*[a]

ketose[b]/polyol[c] substrate pair	k_{cat} (s^{-1})	K_m (mM)	k_{cat}/K_m (mM^{-1} s^{-1})	$-\Delta\Delta G$ (kJ/mol)[e]
D-fructose/D-mannitol	54 ± 2/21 ± 1	25 ± 3/1.2 ± 0.3	2.2/18	−/−
D-xylulose/D-arabinitol	26 ± 2/47 ± 4	133 ± 30/14 ± 4	0.2/3.4	5.9/4.1
D-ribulose/[d]	43 ± 4	9.9 ± 2.4/nd[f]	4.3/nd	−1.7/nd
L-sorbose/D-sorbitol	7.4 ± 1.6/12.8 ± 1.7	647 ± 247/462 ± 100	0.01/0.03	13.4/15.8

[a] Kinetic parameters were obtained from fits to eq 1 or 2, by using initial velocities determined at 25 °C in 50 mM Tris/HCl buffer at pH 7.0 for ketose reduction and pH 9.0 for polyol oxidation. [b] Determined at a constant NADH concentration of 0.2 mM. [c] Determined at a NAD concentration of 2 mM. [d] The putative product is D-arabinitol. [e] Calculated according to the equation $\Delta\Delta G = -RT \ln[(k_{cat}/K_{ketose})/(k_{cat}/K_{fructose})]$ and $-RT \ln[(k_{cat}/K_{polyol})/(k_{cat}/K_{mannitol})]$. [f] Not determined.

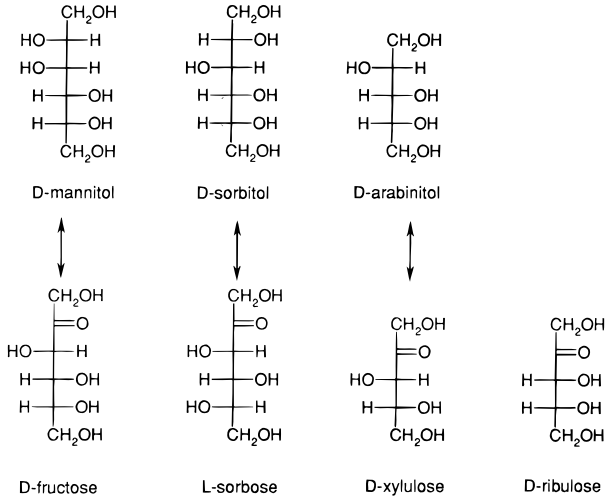

FIGURE 1: Structures of MDH substrates in ketose−polyol interconversion.

Table 3: Kinetic Parameters of MDH from *P. fluorescens*, Compared with Those of SDH from Sheep Liver

parameter	MDH[a]	SDH[b]
k_{catr} (s^{-1})[c]	110 ± 8	178[j]
K_{RO} (mM)[c,d]	(63 ± 12) × 10^{-3}	57.6 × 10^{-1}
K_{IRO} (mM)[e]	360[h]	nd
k_{catr}/K_{RO} (mM^{-1} s^{-1})	175 ± 5[i]	124
k_{cato} (s^{-1})[c]	20.3 ± 1.0	4.8[j]
K_{ROH} (mM)[c]	3.6 ± 0.3	0.96
K_{IROH} (mM)[e]	523 ± 54	nd
k_{cato}/K_{ROH} (mM^{-1} s^{-1})	5.64 ± 0.75	20.0
K_{iNAD} (μM)	109 ± 45	1220
K_{NAD} (μM)	428 ± 68	33
K_{iNADH} (μM)	44 ± 24	6.92
K_{NADH} (μM)	153 ± 35	276
K_{iNAD}/K_{iNADH} ratio	2.5	176
$(k_{catr}/K_{RO})/(k_{cato}/K_{ROH})$ ratio	31	6.2
Haldane[f] ($1/K_{eq}'$)	77.5	1106
log fraction of $1/K_{eq}'$[g]	79	26

[a] Determined at 25 °C and pH 8.2 with 50 mM Tris/HCl buffer. [b] Determined at 23.5 °C and pH 7.4 with 50 mM sodium phosphate buffer (from ref *21*). [c] r, fructose reduction; o, polyol oxidation; RO, D-fructose; ROH, D-mannitol (MDH) and D-sorbitol (SDH). [d] Based on 1% free carbonyl form in solution (*37*). [e] Substrate inhibition constant for inhibition by RO and ROH. [f] Calculated from the experimental parameters for the Haldane relationship of an ordered bireactant mechanism, and the apparent equilibrium constant, K_{eq}', contains the concentration of hydronium ions, according to the equation $K_{eq}' = K_{eq}[H^+]$. [g] Calculated as 100{log(k_{cat}/K ratio)/[log(k_{cat}/K ratio) + log(K_i ratio)]}. [h] Kept constant during nonlinear regression analysis. [i] Calculated according to the term $(\{[\pm k_{catr(o)}]K_{RO(H)} + [\pm K_{RO(H)}]k_{catr(o)}\}/K_{RO(H)}^2)$. [j] Calculated for the SDH protomer from the values for the catalytic SDH tetramer in ref *21*.

true substrate of MDH (and sorbitol dehydrogenase), and therefore, the values for 1/app K_{eq} in Table 3 are based on the free carbonyl species.

Product Inhibition Patterns. Product inhibition by NAD versus NADH and by NADH versus NAD at saturating and nonsaturating concentrations of D-fructose and D-mannitol, respectively, was competitive. NAD was a mixed-type inhibitor versus D-fructose at nonsaturating concentrations of NADH. ATP was a dead-end inhibitor, competitive versus NAD (K_i = 2.2 ± 0.2 mM). D-Mannitol gave a mixed-type inhibition pattern versus D-fructose at nonsaturating concentrations of NADH and was uncompetitive versus NADH at saturating concentrations of D-fructose (K_i = 7.0 ± 0.4 mM). In a double-inhibition experiment at pH 8.2, initial velocities were measured at 0.43 mM NAD which is K_{NAD}, and the D-mannitol concentration was varied at NADH levels of 0, 50, and 100 μM. The extent of substrate inhibition by D-mannitol decreased as the NADH concentration increased. The $K_{Imannitol}$ was 1.5 ± 0.2, 2.1 ± 0.3, and 2.5 ± 0.6 M at 0, 50, and 100 μM NADH, respectively.

Binding of NADH to MDH. This was assessed by fluorescence titration at pH 7.0. The Scatchard plot of the data for NADH binding to MDH gave a dissociation constant, K_d, of 11 ± 2 μM and a number of moles of NADH binding sites per mole of MDH of 1.2 ± 0.2. The K_d value agrees with the K_{iNADH} value determined from kinetic experiments carried out at pH 7.0, by using NADH as a competitive inhibitor versus NAD (not shown).

Physiological Implication of the Kinetic Data. A comparison of the kinetic parameters of MDH and sheep liver SDH (*21*) for the NAD(H)-dependent interconversion of D-fructose and D-mannitol or D-sorbitol, respectively, is shown in Table 3 and as a free energy diagram in Figure 2, where a standard free energy of MDH or SDH, NADH, and D-fructose of zero and a 1.0 M standard state for substrates and products were assumed. Significant differences between the two enzymes are found at the free energies of the binary E−NAD and E−NADH complexes and the ternary E−NADH−ketose complex. The E−NADH complex of MDH is destabilized by 4.6 kJ/mol, relative to the corresponding complex of SDH, whereas the E−NAD complex of MDH is stabilized by 6.0 kJ/mol, reflecting K_i values for NADH and NAD that are 6.3-fold smaller and 11-fold higher than the corresponding dissociation constants of SDH for NADH and NAD. A marked 70-fold difference between MDH and SDH is found when a comparison of the K_{iNAD}/K_{iNADH} ratios for the two enzymes is made. With a value for K_{iNAD}/K_{iNADH} of 2.5, the ratio of catalytic efficiencies, $(k_{catr}/K_{RO})/(k_{cato}/K_{ROH})$, for MDH constitutes a 79% log fraction of the equilibrium constant, compared to only 26% for SDH which has a K_{iNAD}/K_{iNADH} ratio of 176. Note that the K_{iNAD}/K_{iNADH} ratio is not changed significantly for SDH in the pH range of 7.4−8.2 (*38*). Another clear difference between MDH and SDH is the fact that the ternary E−NADH−fructose complex

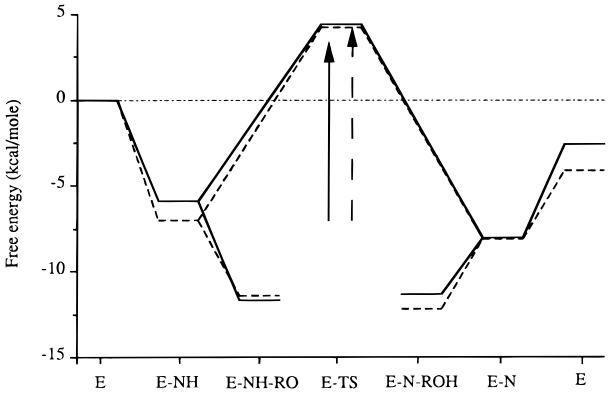

FIGURE 2: Reaction-coordinate diagram comparing the NADH-dependent reduction of D-fructose catalyzed by MDH (solid line) and sheep liver SDH (dashed line), where E is the enzyme, NH and N are NADH and NAD, RO and ROH are D-fructose and D-mannitol or D-sorbitol, and TS is the transition state, respectively. The arrows show $\Delta G^{\ddagger}$ values for the action of MDH (solid line) and SDH (dashed line). See Table 3 for the individual rate and equilibrium constants.

of MDH, compared to that of SDH, is stabilized by an additional 11 kJ/mol, reflecting a 91-fold lower K_{RO} value for MDH. In the direction of fructose reduction, the free energy barrier for MDH is 4 kJ/mol smaller than that of SDH, denoted by the arrows in Figure 2. At a physiological NAD redox ratio of approximately 62 for aerobically grown cells of *Pseudomonas* (*39*), the observed K_{iNAD}/K_{iNADH} ratio of 2.5 determines a concentration of the MDH−NAD complex which is 25 times that of the MDH−NADH complex. If it is considered that approximately 40 μM NADH is present in the bacterial cytoplasm (*39*), the K_{iNADH} value for MDH has been raised to a point where it equals the physiological concentration of the nucleotide which means that the extent of product inhibition of MDH by NADH will be low under these conditions. Interestingly, the analysis of the kinetic data published for MDH from *A. glauca* (*7*) leads to a conclusion similar to that outlined for MDH from *P. fluorescens*. The contribution of the K_{iNAD}/K_{iNADH} ratio (2.55) to the external equilibrium constant is approximately 38% (based on the log fraction), with the remaining 62% being contributed by the $(k_{catr}/K_{RO})/(k_{cato}/K_{ROH})$ ratio.

pH Profiles of the Kinetic Parameters. The pH dependence of the apparent kinetic constants for D-fructose reduction was determined in the pH range of 6.5−10.0 at a constant concentration of NADH (0.2 mM), and the data for varied noninhibitory D-fructose (5−150 mM) at each pH value were fitted to eq 1. The pH dependence of K_{iNADH} was determined from competitive inhibition of NADH versus NAD at a constant D-mannitol concentration of 5 mM ($\approx K_{mannitol}$), and the data were fitted to eq 6. The pH dependence of K_{NADH} was determined at a constant D-fructose concentration (150 mM), by using fits of the data to eq 1. The pH profile of pK_{iNADH} is shown in Figure 3, and data were fitted to eq 9c (Table 4). The value of K_{NADH} was 0.125 ± 0.25 mM and constant in the pH range of 6.5−10.0. Since initial velocities for varied D-fructose concentrations were measured at nonsaturating NADH concentrations and K_{iNADH} is pH-dependent, the thus obtained value for $k_{cat}/K_{fructose}$ at each pH is $(k_{cat}/K_{fructose})/(1 + K_{iNADH}/[NADH])$, where [NADH] is 0.2 mM. The pH profiles of k_{cat} and $k_{cat}/K_{fructose}$ are shown in Figure 4, and values of $k_{cat}/K_{fructose}$ are corrected by $(1 + K_{iNADH}/[NADH])$, using the corresponding data from Figure 3. Note that the pH profile of k_{cat} is valid because K_{NADH} exhibits no pH dependence. Fits of eq 9a to the profiles of log k_{cat} and $\log(k_{cat}/K_{fructose})$ are shown in Table 4.

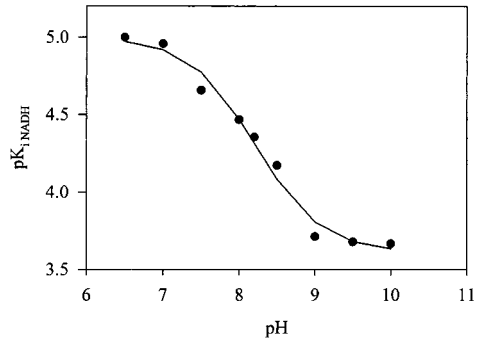

FIGURE 3: pH profile for NADH binding to MDH. pK_{iNADH} was determined from the competitive inhibition vs NAD in direction of D-mannitol oxidation.

Table 4: Values from pH Profiles of the Kinetic Parameters for MDH in Fructose Reduction

parameter	eq fitted	pK_1	pK_2	C^a
$\log(k_{cat}/K_{fructose})$	9a	9.34 ± 0.20		5.30 ± 0.60 mM^{-1} s^{-1}
$\log(k_{cat})$	9a	9.71 ± 0.05		59 ± 2 s^{-1}
pK_{iNADH}[a]	9c	8.23 ± 0.03		Y_L = 9.06 ± 1.80 μM
				Y_H = 251 ± 29 μM
$^D(k_{cat}/K_{fructose})$	9b	5.64 ± 0.15	9.64 ± 0.63	2.52 ± 0.13

[a] For the pK profile, eq 9c was fitted with $Y = 1/K_i$. The values shown for Y_H and Y_L are K_i, not $1/K_i$. The value of K_i at low pH is given first and the value at high pH second.

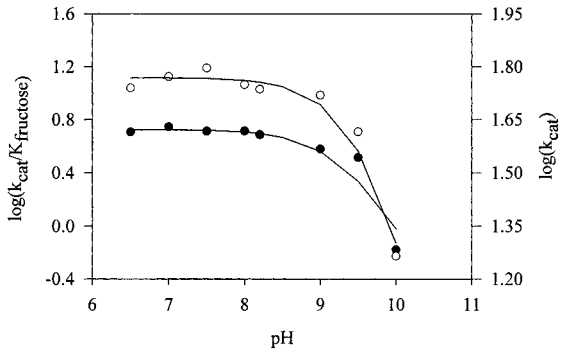

FIGURE 4: pH profile for D-fructose reduction by MDH: (○) log k_{cat} and (●) log $k_{cat}/K_{fructose}$. The units of k_{cat} are s^{-1}, and those of $k_{cat}/K_{fructose}$ are mM^{-1} s^{-1}. The values of $k_{cat}/K_{fructose}$ are corrected for the incomplete saturation of MDH with NADH (see the text).

Deuterium Isotope Effects. Primary kinetic deuterium isotope effects were measured in the pH range of 6.5−10.0 by a direct comparison of the initial velocities obtained with varied D-fructose concentrations (10−150 mM) and a constant (4*S*)-[4-D]NADD concentration (0.2 mM) and initial velocities obtained with varied (4*S*)-[4-D]NADD concentrations (0.05−0.25 mM) and a constant D-fructose concentration (150 mM). The results obtained from a fit of eq 5 to the experimental data are shown in Figure 5. There is a significant primary isotope effect on k_{cat} and k_{cat}/K over the pH range of 6.5−9.5, consistent with a significant contribution of hydride transfer to rate limitation for the overall reaction as well as the catalytic cascade for this pH range. Note that the full isotope effect on $k_{cat}/K_{fructose}$ is observed despite the incomplete saturation of MDH with NADH (*22*).

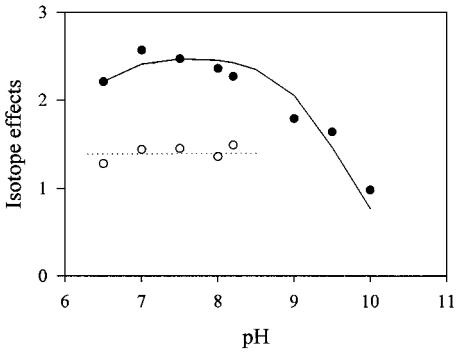

FIGURE 5: pH variation of the primary deuterium isotope effect in D-fructose reduction, using (4*S*)-[4-D]NADD as the coenzyme. $^{D}(k_{cat}/K_{fructose})$ values (●) were determined at 0.2 mM coenzyme. $^{D}k_{cat}$ values (○) were determined at a constant concentration of D-fructose (500 mM) with the (4*S*)-[4-D]NADD concentration being varied.

Results of a fit of eq 9b to $^{D}(k_{cat}/K_{fructose})$ are shown in Table 4. The isotope effect on k_{cat} is constant (1.44 ± 0.2) in the pH range of 6.5−8.2 (Figure 5). $^{D}k_{cat}$ values obtained for varied D-fructose and varied (4*S*)-[4-D]NADD concentrations were consistent. The isotope effects on k_{cat}/K_{NADH} at pH 7.0, 8.2, and 9.0 were 1.08 ± 0.15, 1.02 ± 0.10, and 1.01 ± 0.10, respectively. Despite a standard error of approximately 10%, repeated determinations of $^{D}(k_{cat}/K_{NADH})$ showed that at pH 7.0 but not at pH 8.2 and 9.0, the isotope effect on k_{cat}/K_{NADH} was significantly different from unity.

Solvent Isotope Effects. The solvent isotope effects for MDH on $k_{cat}/K_{fructose}$ and k_{cat} were determined at pH(D) 7.0. There was a significant isotope effect on both kinetic constants, $^{D_2O}k_{cat} = 1.92 \pm 0.17$ and $^{D_2O}(k_{cat}/K_{fructose}) = 2.56 \pm 0.29$, indicating that the proton transfer rate contributes to rate limitation of the catalytic sequence as well as to the overall reaction at this pH.

DISCUSSION

Mannitol dehydrogenases constitute a recently identified subfamily within the heterogeneous family of long-chain alcohol dehydrogenases (*9*). They share no entire-chain similarities with members of other alcohol dehydrogenase families, and even a lack of segment similarity, apart from residues probably involved in coenzyme binding, was reported (*9*). Given the structural differences with respect to well-known alcohol/polyol dehydrogenases (see refs *13*, *15*, *16*, and *35*), it seems interesting to investigate functional and mechanistic properties of mannitol dehydrogenases which have, hitherto, not been described. Here, we have studied in detail the kinetic mechanism of MDH from *P. fluorescens* and present an analysis of the kinetic data with regard to enzyme function under prevailing physiological reaction conditions.

Kinetic Mechanism. A number of experiments indicate that the kinetic mechanism of MDH is ordered with kinetically significant central ternary complexes, as shown in eq 12.

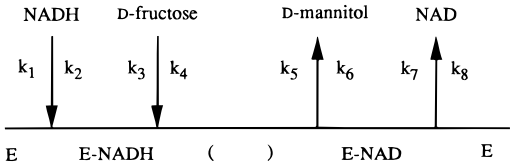

(12)

Product inhibition studies together with binding studies suggest that NADH and NAD bind to free MDH, followed by D-fructose and D-mannitol, respectively. Uncompetitive substrate inhibition by D-fructose indicates the formation of a dead-end ternary MDH−NAD−fructose complex which is characteristic of an ordered mechanism but not of a random mechanism. At pH 8.2, there is a much larger isotope effect on $k_{cat}/K_{fructose}$ than on k_{cat}/K_{NADH} which suggests that NADH does not dissociate rapidly from the ternary MDH−NADH−fructose complex which is in agreement with eq 12. Because there is only one isotope-sensitive step in eq 12, we can write (*22*)

$$^{D}(k_{cat}/K_{fructose}) = (^{D}k_5 + c_f + {}^{D}K_{eq}c_r)/(1 + c_f + c_r) \quad (13)$$

$$^{D}k_{cat} = (^{D}k_5 + c_{vf} + {}^{D}K_{eq}c_r)/(1 + c_f + c_r) \quad (14)$$

where $^{D}k_5$ is the isotope effect on k_5 and c_f and c_r are the commitments in the forward and reverse direction, respectively. The constant c_{vf} is a comparison of the rate constant for the isotope-dependent step to all other forward unimolecular steps (*22*). $^{D}K_{eq}$ is the equilibrium isotope effect (*22*). Cook and Cleland (*23*) have shown that the isotope effect on k_{cat}/K for the substrate which adds first in a strictly ordered bi bi kinetic mechanism must be equal to unity. The reason is that at a saturating concentration of the second substrate the forward commitment factor will become infinite, and therefore, the isotope effect on k_{cat}/K is completely masked. Accordingly, MDH follows a strictly ordered mechanism at pH 8.2 and 9.0. A small but possibly real isotope effect on k_{cat}/K_{NADH} is seen at pH 7.0, which indicates that NADH may be released slowly from the central complex at pH 7.0. Given that D-fructose is not sticky (see below) and using a $^{D}(k_{cat}/K_{fructose})$ of 2.57, the value of 1.08 for $^{D}(k_{cat}/K_{NADH})$ corresponds to release of NADH from MDH−NADH−fructose at a rate that is approximately 19 times the rate of reaction to give D-mannitol (cf. ref *23*). Therefore, some degree of randomness is present at pH 7.0 which is the pH optimum for D-fructose reduction, and the mechanism may be truly random at this pH with a strongly preferred pathway in which NADH binds before D-fructose.

Isomerization of the MDH−NAD Complex. The kinetic constants in Table 3 allow the calculation of k_2 in eq 12 as (*40*)

$$k_2 = k_{catr}K_{iNADH}/K_{NADH} = 32\ s^{-1}$$

When the fact that k_{cat} in D-mannitol oxidation is 20 s^{-1} is taken into account, then k_2 appears to be the major rate-limiting step for the overall reaction in this direction. At saturating concentrations of D-mannitol and NAD, 62% of the enzyme will thus be in the MDH−NADH complex. According to eq 12, the ratio of kinetic constants, k_{catr}/K_{NADH}, equals the rate constant k_1. A value for k_1 of 0.72×10^6 M^{-1} s^{-1}, calculated by using the kinetic constants in Table 3, is not in the expected range of 10^8−10^9 M^{-1} s^{-1} for a diffusion-limited on-rate for NADH binding (*41*). NADH binding could therefore be a two-step process which appears as a single step. An analysis similar to that shown for k_2 above was carried out for k_7 in eq 12 and yields a value of 5 s^{-1} for this rate constant. However, k_{cat} in D-fructose reduction is 110 s^{-1}, and k_7 must be larger than this number.

If however the MDH−NAD complex isomerizes (eq 15)

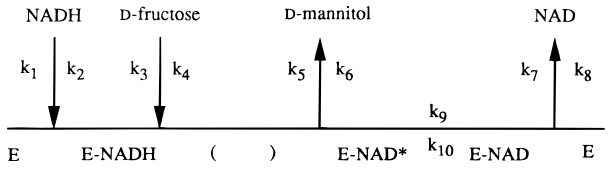

(15)

then (*42*)

$$k_{cato}K_{iNAD}/K_{NAD} = k_7k_9k_{10}/[(k_7 + k_9)(k_9 + k_{10})] \quad (16)$$

Because k_7 and k_9 must both exceed 110 s^{-1}, the expression in eq 16 equals k_{10} which is then 5 s^{-1}. The k_{cat} of 20 s^{-1} in D-mannitol oxidation requires that all first-order rate constants in this direction be larger than this value, and therefore, 5 s^{-1} cannot be the true value for k_{10}. We have no way of knowing what additional reaction steps are responsible for $k_{cato}K_{iNAD}/K_{NAD}$ giving a value of <20 s^{-1}. One explanation could be that MDH and NAD form a nonproductive dead-end complex, which blocks the reaction and has a dissociation constant that is smaller than that of the active MDH−NAD complex. In this case, the observed K_{iNAD} will be smaller than k_7/k_8 and reflect the nonproductive binding of NAD. The occurrence of an inactive enzyme−NAD complex which cannot combine with D-mannitol productively is supported by the pattern of substrate inhibition by D-mannitol. Uncompetitive substrate inhibition in an ordered reaction (see eq 12) is generally expected to result from a combination of D-mannitol with MDH−NADH. In the case of MDH, kinetic evidence does not favor the formation of a dead-end MDH−NADH−mannitol complex, as follows. When NAD was added to the assay in a constant concentration equal K_{NAD} and no NADH was present, substrate inhibition was observed for D-mannitol as the varied substrate. Since under these conditions no MDH−NADH will be present, substrate inhibition must result from a combination of MDH−NAD with D-mannitol. Double-inhibition experiments in which increasing concentrations of NADH were added to the assay showed that the presence of NADH reduces the extent of substrate inhibition by D-mannitol. Therefore, substrate inhibition does not result from a combination of MDH−NADH and D-mannitol. Binding of D-mannitol to the inactive MDH−NAD would prevent the isomerization to the productive MDH−NAD from taking place, and thus produces substrate inhibition by D-mannitol. The rate constant ratio k_{cato}/K_{NAD} of 0.47×10^5 M^{-1} s^{-1}, calculated from the data in Table 3, is more than 2 orders of magnitude lower than the expected on rate for nucleotide binding which supports a mechanism involving isomerization of the MDH−NAD complex.

Catalytic Mechanism: pH Profiles and Isotope Effects. The pH profile of pK_{iNADH} is a wave, showing a titratable group in the free enzyme which has an apparent pK of 8.23 and must be protonated for optimal binding of NADH. The pH variation of log $k_{cat}/K_{fructose}$ shows a single enzymic group in the MDH−NADH complex with an apparent pK of 9.34, which must be protonated for substrate binding or catalysis. The pH profile of log k_{cat} decreases above an apparent pK of 9.71. The fact that the same groups do not appear in the pH profiles of log $k_{cat}/K_{fructose}$ and log k_{cat} could have two plausible mechanistic explanations. (1) Binding of D-fructose to MDH−NADH to form the ternary complex locks the enzyme in the correct state of protonation. (2) The outward shift by approximately 0.37 pH unit in the pH profile of k_{cat}, relative to $k_{cat}/K_{fructose}$, occurs because only if catalysis is slowed by 0.37 log unit, which is approximately 2.3-fold, does it become equal to another slow step outside $k_{cat}/K_{fructose}$, likely NAD release (see below). If it is assumed that D-fructose can bind to the protonated and unprotonated MDH−NADH complex, but only the protonated form is catalytically competent, then the observed pK shift for the variation of log k_{cat} with pH, relative to that of log($k_{cat}/K_{fructose}$), would be (*43*)

$$\Delta pK = \log[1 + (k_{react}/k_{off})] \quad (17)$$

where k_{react} and k_{off} are net rate constants for reaction and product release, respectively.

The pH dependence of the isotope effects on $k_{cat}/K_{fructose}$ indicates that D-fructose is not sticky at the pH optimum of 7.0; i.e., it reacts slower to give products than it dissociates from the ternary complex (*22*). The $^D(k_{cat}/K_{fructose})$ values decrease from 2.57 at pH 7.0 to 0.98 at pH 10.0. If D-fructose were sticky, $^D(k_{cat}/K_{fructose})$ would be expected to increase above the pK of 9.34 as the net rate of the hydride-transfer step decreased relative to the rate of release of D-fructose (*22*, *44*, *45*). Because D-fructose is not sticky, the pK value of 9.34 observed in the pH profile of $k_{cat}/K_{fructose}$ represents probably the true pK for the ionizable enzymic group in the productive MDH−NADH complex. The results imply furthermore that the observed value for $^D(k_{cat}/K_{fructose})$ of 2.57 at pH 7.0 is equal to the intrinsic isotope effect reduced only by internal commitments (eq 13); i.e., $^Dk_5$ in eq 12 equals 2.57.

Since a value of $^Dk_{cat}$ that is less than $^D(k_{cat}/K_{fructose})$ is observed at the pH optimum for D-fructose reduction, a reaction step outside the catalytic sequence, likely the rate of release of NAD, is partly responsible for rate limitation of the overall reaction at this pH. By using a simplified model (eq 18) which does not consider commitments in the reverse reaction (*23*)

$$^Dk_{cat} = {}^Dk_5 + c_{vf}/(1 + c_{vf}) \quad (18)$$

and values for $^Dk_{cat}$ of 1.44 and $^Dk_5$ of 2.57, we can estimate from the lumped parameter, c_{vf}, that the rate of NAD release at pH 7.0 is approximately 2.6 times slower than the catalytic sequence represented by k_5. The constant value of $^Dk_{cat}$ between pH 6.5 and 8.0 indicates that the contribution of the hydride-transfer rate to rate limitation for the entire reaction is constant for this pH range, relative to that of the isotope-independent step of NAD release.

The observation of a significant solvent isotope effect on k_{cat} and $k_{cat}/K_{fructose}$ at pH(D) 7.0 indicates that the rate of proton transfer contributes to rate limitation of the overall reaction as well as the catalytic cascade. Since similar values for $^D(k_{cat}/K_{fructose})$ and $^{D_2O}(k_{cat}/K_{fructose})$ were observed, hydride transfer and proton transfer could occur in a concerted or stepwise manner. If we assume a value for the intrinsic isotope effect on hydride transfer (^Dk) between 5.3 (*46*) and 6.5 (*47*) and for proton transfer (^{D_2O}k) of 8 (*48*), then for a stepwise mechanism with a $^Dk_5$ of 2.57 and a $^{D_2O}k_5$ of 2.56 at pH 7.0, the simple calculation, e.g., $(^Dk_5 - 1)/(^Dk - 1)$

(*49*), suggests 29−36% rate limitation by hydride transfer and about 22% rate limitation by proton transfer, with the remainder contributed by other steps comprising $k_{cat}/K_{fructose}$. With a rate of hydride transfer at pH 7.0 that is about 29−36% rate-limiting for $k_{cat}/K_{fructose}$ and 2.6 times faster than the rate of NAD release at this pH, a pK shift of 0.9 pH unit, equal to $\Delta pK = \log[1 + (2.6/0.36)]$, in the pH profile for k_{cat}, relative to that for $k_{cat}/K_{fructose}$, would be expected. Therefore, the observed outward shift by approximately 0.4 pH unit could be caused by the pH-dependent slowing of catalysis, relative to NAD release.

The isotope effect on $k_{cat}/K_{fructose}$ decreases above an apparent pK of 9.64 and becomes 0.98 ± 0.15 at pH 10.0. However, it was impossible to determine with sufficient accuracy whether, above pH 10.0, $^{D}(k_{cat}/K_{fructose})$ decreases to a limiting value of 1.00 or the equilibrium isotope effect for the NADH-dependent reduction of a ketone, which is 0.85 (*50*, *51*). Cook and Cleland developed theory for the pH variation of isotope effects in enzyme-catalyzed reactions (*24*, *25*). They showed that if the isotope- and the pH-dependent step are the same, isotope effects on k_{cat}/K and k_{cat} will become equal at high or low pH where k_{cat}/K and k_{cat} decrease, and for a slow nonsticky substrate, the isotope effect on k_{cat}/K is expected to exhibit no variation with pH (*24*). If the isotope-dependent step is not pH-dependent, then the isotope effects will decrease at pH values where the pH-dependent step becomes completely rate-limiting, either to 1.00 or the equilibrium isotope effect, depending on whether the pH-dependent step occurs before or after the isotope-dependent one (*25*). Since $^{D}(k_{cat}/K_{fructose})$ decreases above a pK of 9.64 to 1.00 (or K_{eq}), the isotope-dependent step for MDH-catalyzed D-fructose reduction is not pH-dependent. Whether the isotope-independent reaction step whose rate is slowed at high pH, such as structural reorganizations of the ternary enzyme−reactant complex, for example, occurs before the hydride transfer step or after catalysis is complete remains uncertain for MDH. In the case of yeast and liver alcohol dehydrogenase in the direction of carbonyl reduction (*25*), the pH-dependent but isotope-independent step occurred after the isotope-dependent one; hence, isotope effects on $k_{cat}/K_{substrate}$ and k_{cat} decreased to $^{D}K_{eq}$ at high pH. For MDH, the pH dependence of $^{D}k_{cat}$ was determined in the pH range of 6.5−8.2, where $^{D}k_{cat}$ was constant. It is likely, however, that $^{D}k_{cat}$ will decrease to a value of 1.00 or $^{D}K_{eq}$ at high pH, which is above a pK of approximately 9.6−9.7.

Kinetic Parameters and the Physiological Role of MDH, Compared with Those of SDH. A comparison of the kinetic properties of bacterial MDH and mammalian SDH led to a clear picture of the physiological role of MDH. SDH was chosen because it catalyzes a reaction very similar to that of MDH, but its physiological function was presumed to be diametrically opposed to that of the bacterial enzyme. SDH mediates the oxidation of D-sorbitol in a "low-flux" metabolic bypass and may be involved in detoxification metabolism of certain alcohols (*19*−*21*). According to Grimshaw (*52*), a broad spectrum alcohol dehydrogenase designed to operate in the thermodynamically unfavorable direction of alcohol oxidation would ideally evolve to a point where the contribution of the $(k_{catr}/K_{RO})/(k_{cato}/K_{ROH})$ ratio to the expression of the external equilibrium constant is minimal. In agreement with this notion, the K_{iNAD}/K_{iNADH} ratio for SDH of 176 is roughly matched to the prevailing NAD redox ratio in the liver cytosol of 725 (*53*), which means that a drastic further increase for the K_i ratio, with a concomitant decrease of the $(k_{catr}/K_{RO})/(k_{cato}/K_{ROH})$ ratio, would result in significant product inhibition by NADH. Because of rate-limiting dissociation of NADH (*21*) which reflects the tight binding of NADH, SDH exhibits a turnover number which is constant across a series of polyol substrates, differing in the number of carbon atoms as well as in the orientation of the hydroxyl groups at individual carbon atoms (*26*).

The MDH exhibits a behavior which is markedly different from that of SDH. It utilizes differential binding (*54*) of D-mannitol versus D-fructose as an enzymic mechanism to (1) shift the bound-state equilibrium constant toward alcohol oxidation and (2) increase k_{cat} in the oxidative direction, up to a point where dissociation of NADH becomes largely rate-limiting for the overall reaction (see below). However, in contrast to SDH which has a net rate constant for the dissociation of NADH from the enzyme-NADH complex of 4.5 s^{-1}, the corresponding rate constant for MDH is 32 s^{-1}. Efficient use of the intrinsic binding energy of the polyol substrate as a means for maximizing the turnover number makes perfect sense for a catalyst designed to operate with high fluxional efficiency in the oxidative direction and is in accordance with a physiological role of MDH in mainstream catabolism of D-mannitol by *P. fluorescens*. Relative to SDH, the contribution to transition-state stabilization of noncovalent interactions of the binary MDH−NAD complex with nonreacting portions of the substrate is clearly more important for MDH which is reflected by a rather narrow spectrum of polyols, D-mannitol and D-arabinitol, which are converted by MDH at appreciable rates. It is noteworthy that D-sorbitol, for which a loss of binding energy of approximately 16 kJ/mol was observed relative to D-mannitol, is probably not a physiological substrate of MDH. This finding is in good agreement with the occurrence of MDH and SDH activities in *P. fluorescens* and related microorganisms. Brünker et al. (*55*) have recently characterized a number of genes which are involved in the utilization of polyols by *P. fluorescens* and seem to be organized in a single operon. Two genes within the operon encode an unspecific D-fructokinase and a specific D-xylulokinase which together will ensure the catabolism of the ketose products derived from MDH action. The genetic evidence (*55*) together with the kinetic evidence obtained in this work suggests that because of its dual specificity concerning the polyol substrate MDH will catalyze the first step of metabolic pathways in *P. fluorescens* designed to enable the utilization of D-mannitol and D-arabinitol for growth and energy.

ACKNOWLEDGMENT

The kind help of Dr. M. Puchberger (Institute of Chemistry, BOKU) with NMR measurements is gratefully acknowledged. Drs. T. Prohaska and C. Latkoczy (Institute of Chemistry, BOKU) are thanked for carrying out the metal analysis of MDH.

SUPPORTING INFORMATION AVAILABLE

A table describing the purification of recombinant wild-type MDH and three figures showing SDS−PAGE of purified MDH, double-reciprocal plots of initial velocity data, and Scatchard analysis of NADH binding to MDH. This

material is available free of charge via the Internet at http://pubs.acs.org.

REFERENCES

1. Loescher, W. H. (1987) *Physiol. Plant. 70*, 553−557.
2. Stoop, J. M. H., Chilton, W. S., and Pharr, D. M. (1996) *Phytochemistry 43*, 1145−1150.
3. Williamson, J. D., Stoop, J. M. H., Massel, O., Conkling, A. A., and Pharr, D. M. (1995) *Proc. Natl. Acad. Sci. U.S.A. 92*, 7148−7152.
4. Martinez, G., Barker, H. A., and Horecker, B. L. (1963) *J. Biol. Chem. 238*, 1598−1603.
5. Ueng, S. T.-H., Hartanowicz, P., Lewandoski, C., Keller, J., Holick, M., and McGuiness, E. T. (1976) *Biochemistry 15*, 1743−1749.
6. Yamanaka, K. (1975) *Methods Enzymol. 41*, 138−142.
7. Ueng, S. T.-H., and McGuiness, E. T. (1977) *Biochemistry 16*, 107−111.
8. Brünker, P., Altenbuchner, J., Kulbe, K. D., and Mattes, R. (1998) *Biochim. Biophys. Acta 1351*, 157−167.
9. Schneider, K.-H., Giffhorn, F., and Kaplan, S. (1993) *J. Gen. Microbiol. 139*, 2475−2484.
10. Haltrich, D., Nidetzky, B., Miemietz, G., Gollhofer, D., Lutz, P., Stolz, P., and Kulbe, K. D. (1995) *Biocatal. Biotransform. 14*, 31−45.
11. Schneider, K.-H., and Giffhorn, F. (1989) *Eur. J. Biochem. 184*, 15−19.
12. Jörnvall, H., Persson, B., and Jeffery, J. (1987) *Eur. J. Biochem. 167*, 195−201.
13. Persson, B., Zigler, S., Jr., and Jörnvall, H. (1994) *Eur. J. Biochem. 226*, 15−22.
14. Persson, B., Krook, M., and Jörnvall, H. (1991) *Eur. J. Biochem. 200*, 537−543.
15. Jörnvall, H., Persson, B., Krook, M., Atrian, S., Gonzalez-Duarte, R., Jeffery, J., and Ghosh, D. (1995) *Biochemistry 34*, 6003−6013.
16. Jez, J. M., Bennett, M. J., Schlegel, B. P., Lewis, M., and Penning, T. M. (1997) *Biochem. J. 326*, 625−636.
17. Persson, B., Jeffery, J., and Jörnvall, H. (1991) *Biochem. Biophys. Res. Commun. 177*, 218−223.
18. Persson, B., Jörnvall, H., Wood, I., and Jeffery, J. (1991) *Eur. J. Biochem. 198*, 485−491.
19. Lindstad, R. I., and McKinley-McKee, J. S. (1993) *FEBS Lett. 300*, 31−35.
20. Lindstad, R. I., Köll, P., and McKinley-McKee, J. S. (1998) *Biochem. J. 330*, 479−487.
21. Lindstad, R. I., Hermansen, L. F., and McKinley-McKee, J. S. (1992) *Eur. J. Biochem. 210*, 641−647.
22. Cleland, W. W. (1990) in *The Enzymes* (Sigman, D. S., and Boyer, P. D., Eds.) Vol. 19, pp 99−158, Academic Press, San Diego.
23. Cook, P. F., and Cleland, W. W. (1981) *Biochemistry 20*, 1790−1796.
24. Cook, P. F., and Cleland, W. W. (1981) *Biochemistry 20*, 1797−1805.
25. Cook, P. F., and Cleland, W. W. (1981) *Biochemistry 20*, 1805−1816.
26. Barski, O. A., Gabbay, K. H., Grimshaw, C. E., and Bohren, K. M. (1995) *Biochemistry 34*, 11264−11275.
27. Grimshaw, C. E., Bohren, K. M., Lai, C.-J., and Gabbay, K. H. (1995) *Biochemistry 34*, 14356−14365.
28. Grimshaw, C. E., Bohren, K. M., Lai, C.-J., and Gabbay, K. H. (1995) *Biochemistry 34*, 14374−14384.
29. Kiefer, P. M., Grimshaw, C. E., and Whiteley, J. M. (1997) *Biochemistry 36*, 9438−9445.
30. Moses, V., and Ferrier, R. J. (1962) *Biochem. J. 83*, 8−14.
31. Huwig, A., Danneel, H.-J., and Gifforn, F. (1994) *J. Biotechnol. 32*, 309−315.
32. Mostad, S. B., and Glasfeld, A. (1993) *J. Chem. Educ. 70*, 504−506.
33. Orr, G. A., and Blanchard, J. S. (1984) *Anal. Biochem. 142*, 232−234.
34. Feldmann, I., Tittes, W., Jakubowski, N., Stuewer, D., and Giessmann, U. (1994) *J. Anal. Atom. Spectrosc. 9*, 1007−1014.
35. Jeffery, J., and Jörnvall, H. (1988) *Adv. Enzymol. 61*, 47−106.
36. Eklund, H., Horjales, E., Jörnvall, H., Bränden, C.-I., and Jeffery, J. (1985) *Biochemistry 24*, 8005−8012.
37. Collins, P., and Ferrier, R. (1995) *Monosaccharides*, p 41, Wiley, New York.
38. Lindstad, R. I., and McKinley-McKee, J. S. (1995) *Eur. J. Biochem. 233*, 891−898.
39. Bae, W., and Rittman, B. E. (1996) *Biotechnol. Bioeng. 49*, 690−699.
40. Segel, I. (1993) *Enzyme Kinetics*, Wiley Classics Library Edition, pp 588−589, Wiley Interscience, New York.
41. Fersht, A. R. (1985) *Enzyme Structure and Mechanism*, Freeman, New York.
42. Cleland, W. W. (1963) *Biochim. Biophys. Acta 67*, 104−137.
43. Cleland, W. W. (1977) *Adv. Enzymol. 45*, 273−387.
44. Grimshaw, C. E., and Cleland, W. W. (1981) *Biochemistry 20*, 5650−5655.
45. Grimshaw, C. E., Cook, P. F., and Cleland, W. W. (1981) *Biochemistry 20*, 5655−5661.
46. Hermes, J. D., Roeske, C. A., O'Leary, M. H., and Cleland, W. W. (1982) *Biochemistry 21*, 5106−5114.
47. Scharschmidt, M., Fischer, M. A., and Cleland, W. W. (1984) *Biochemistry 23*, 5471−5478.
48. Xue, L., Talalay, P., and Mildvan, A. S. (1991) *Biochemistry 30*, 10858−10865.
49. Northrop, D. B. (1975) *Biochemistry 14*, 2644−2651.
50. Cook, P. F., Blanchard, J. S., and Cleland, W. W. (1980) *Biochemistry 19*, 4853−4858.
51. Cleland, W. W. (1980) *Methods Enzymol. 64*, 104−125.
52. Grimshaw, C. E. (1992) *Biochemistry 31*, 10139−10145.
53. Veech, R. L. (1987) in *Pyridine Nucleotide Coenzymes: Chemical, Biochemical and Medical Aspects* (Dolphin, D., Poulson, R., and Avramovic, J., Eds.) Vol. II, Part B, pp 79−104, Wiley, New York.
54. Jencks, W. P. (1975) *Adv. Enzymol. 43*, 219−410.
55. Brünker, P., Altenbuchner, J., and Mattes, R. (1998) *Gene 206*, 117−126.

BI990327G